**Climate Dynamics manuscript No.**
(will be inserted by the editor)

# Subtropical-tropical pathways of spiciness anomalies and their impact on equatorial Pacific temperature

**Mathias Zeller · Shayne McGregor · Erik van Sebille · Antonietta Capotondi · Paul Spence**

Received: date / Accepted: date

**Abstract** Understanding mechanisms of tropical Pacific decadal variability (TPDV) is of high importance for differentiating between natural climate variability and human induced climate change as this region sustains strong global teleconnections. Here, we use an ocean general circulation model along with a Lagrangian tracer simulator to investigate the advection of density compensated temperature anomalies ("spiciness mechanism") as a potential contributor to TPDV during the 1980-2016 period. Consistent with observations, we find the primary regions of spiciness generation in the eastern subtropics of each hemisphere. Our results indicate that 75% of the equatorial subsurface water originates in the subtropics, of which two thirds come from the Southern hemisphere. We further show two prominent cases where remotely generated spiciness anomalies are advected to the equatorial Pacific, impacting subsurface temperature. The relative contribution of Northern versus Southern Hemisphere prominence and/or interior versus western boundary pathways depends on the specific event. The anomalously warm case largely results from advection via the Southern hemisphere interior (65%), while the anomalously cold case largely results from advection via the Northern hemisphere western boundary (48%). The relatively slow travel times from the subtropics to the equator (>4 years) suggests that these spiciness anomalies underpin a potentially predictable contribution to TPDV. However, not all decadal peaks in

M. Zeller
School of Earth, Atmosphere and Environment, Monash University, Melbourne, Australia
Tel.: +61-990-54892
E-mail: mathias.zeller@monash.edu

S. McGregor
School of Earth, Atmosphere and Environment, Monash University, Melbourne, Australia

E. van Sebille
Institute for Marine and Atmospheric Research, Utrecht University, Utrecht, Netherlands

A. Capotondi
Physical Sciences Division, NOAA Earth System Research Laboratory, Boulder, Colorado, USA

P. Spence
School of Geosciences, University of Sydney, Sydney, Australia

equatorial spiciness can be explained by remotely generated spiciness anomalies. In those cases, we propose that spiciness anomalies are generated in the equatorial zone through changes in the proportion of Northern/Southern hemisphere source waters due to their different mean spiciness distribution.

**Keywords** Tropical Pacific · Decadal Variability · Ocean Spiciness

## 1 Introduction

In recent decades, a lot of effort has been put into the understanding of the Pacific Decadal Oscillation (PDO) which has its dominant expression in the extratropical North Pacific. A summary of the findings and the current state of knowledge is provided by Newman et al. (2016). The PDO along with its often recognised Pacific-wide sea surface temperature (SST) manifestation, the Interdecadal Pacific Oscillation (IPO), both display a clear decadal SST signal in the tropical Pacific. However, the origin of this tropical SST signal remains unclear. Yet, the decadal SST changes in the tropical Pacific have been found to be of great importance. Low-frequency changes in the tropical Pacific set the background of the El Niño - Southern Oscillation (ENSO) and have been associated with changes in the frequency, intensity (Zhao et al., 2016), flavour (Freund et al., 2019), and predictability (Neske and McGregor, 2018) of ENSO events. Moreover, the recent negative phase of the IPO was shown to explain a large portion of the slow-down in global surface warming at the beginning of the $21^{st}$ century (Kosaka and Xie, 2013; England et al., 2014). Considering the unique impact of the tropical Pacific on the global climate, a better understanding of the drivers of the tropical Pacific decadal variability would be of great scientific and societal value.

Various theories exist that aim to identify the drivers that generate tropical Pacific decadal variability. These drivers can broadly be separated into two main categories: i) local drivers that reside in the tropical Pacific and ii) remote drivers that impact the tropics via teleconnections.

Local drivers are largely related to the occurrence of ENSO. Vimont (2005) suggests that due to ENSO irregularities, simple averages over decadal periods with more El Niño events than La Niña events would imprint an El Niño-like decadal signal in the tropical Pacific and vice versa. Another explanation is given by Rodgers et al. (2004), who argue that the dynamical nonlinearities associated with ENSO lead to a rectification of the interannual ENSO variations into the mean state. While the explanation by Vimont (2005) relies on the difference in the number of El Niño/La Niña events during a given decadal period, purely due to sampling variability, which may result in an El Niño-like or La Niña-like mean state in that epoch, the explanation by Rodgers et al. (2004) relies on the nonlinear rectification of ENSO into the mean state and thus requires nonlinear dynamical processes.

In terms of remote drivers, various studies have focused on the contribution of atmospheric dynamics to tropical Pacific decadal variability. On the one hand, this contribution can occur due to extratropical-tropical interactions within the Pacific region via changes in the strength of the Hadley circulation (Barnett et al., 1999) or via North and South Pacific meridional modes (Di Lorenzo et al., 2015),

and on the other hand due to inter-basin teleconnections from the Atlantic or Indian Ocean via changes in the zonal Walker circulation (McGregor et al., 2014; Chikamoto et al., 2016).

In the ocean, the Pacific subtropical cells (STCs) are the oceanic counterpart to the atmospheric Hadley cells connecting the subtropics with the equator (McCreary Jr and Lu, 1994; Liu et al., 1994; Lee and Fukumori, 2003; Schott et al., 2004; Capotondi et al., 2005). As the STCs regulate the supply of cold subsurface water to the equator, they have been associated with decadal changes in the tropical Pacific through several different mechanisms. Kleeman et al. (1999) proposed that long-term variations in the STC strength have the potential to modulate the tropical Pacific climate through changes in the rate of equatorial upwelling. In a recent study, Zeller et al. (2019) suggested that this mechanism is dominated by the changes in the Southern hemisphere STC strength. The resulting hemispheric asymmetry of STC transports may critically modulate this mechanism given the difference in mean subsurface ocean temperature between the Northern and Southern extratropiccal regions. An alternative mechanism is based on the advection of temperature anomalies from the mid-latitudes to the tropics with the mean STC circulation (Gu and Philander, 1997; Giese et al., 2002; Zhang et al., 1998). Temperature anomalies alone, however, have been shown to be of minor importance for the tropical Pacific as the examined temperature anomalies subducted in the central North Pacific, where the decadal signal is strongest, largely decay before reaching the equator (Schneider et al., 1999a,b; Hazeleger et al., 2001). The relative importance of each of the above mentioned mechanisms in generating the observed decadal signal is still unknown.

Schneider (2000) proposed a subtle alternative to the Gu and Philander (1997) hypothesis, whereby advection of ocean spiciness anomalies replace the proposed temperature advection mechanism. Ocean spiciness has been defined by Munk (1981) as density compensated anomalies of temperature and salinity. On a layer of constant density, hot and salty water is defined as being more spicy than cool and fresh water. Density compensated temperature (spiciness) anomalies are fundamentally different from thermal anomalies generated by subduction as the ones analysed by Gu and Philander (1997) and Schneider et al. (1999a). Subducted thermal anomalies modify the vertical density structure of the ocean by uplifting/suppressing the mean thermocline and are of diabatic origin. Spiciness anomalies, on the other hand, are density-compensated and do therefore not affect the density profile. They behave like passive tracers and propagate with the mean circulation along isopycnal surfaces without significant dissipation.

Spiciness can be generated by two distinct mechanisms. i) Through anomalous advection across mean temperature gradients as explained by Schneider (2000). In this case, anomalous winds and wind stress curl force anomalous ocean currents which shift temperature gradients on isopycnals away from their mean position. This shift causes temperature anomalies on isopycnals, hence spiciness anomalies. As this mechanism is based on anomalous advection it can be referred to as a subset of $v'\overline{T}$, where $v'$ indicates the anomalous flow orthogonal to the mean gradient of spiciness $\overline{T}$. ii) Through convective mixing at the base of the surface mixed layer, as explained by Yeager and Large (2007). The generation occurs predominantly

during winter when stratification is weak in the subtropical and mid-latitude regions where unstable vertical salinity gradients prevail. These conditions allow for enhanced vertical mixing which causes a sharp gradient of both temperature and salinity at the base of the mixed layer. Through the penetrative mixing at the base of the convective boundary layer, a shallow layer of strongly density compensated water with various combinations of temperature and salinity properties is formed between the mixed layer above and the permanent pycnocline below. This layer is the region where spiciness anomalies are generated. In this case, the mechanism does not rely on anomalous currents so it can be referred to as a subset of $\overline{v}T'$. In both cases the generated spiciness anomalies are subsequently advected away by the ocean circulation.

Observations substantiate the existence of spiciness anomalies in the mid-latitudes of all ocean basins (Yeager and Large, 2007) as well as in the tropical Pacific Ocean (Li et al., 2012). The model study by Schneider (2000) suggests the existence of a decadal mode of coupled ocean-atmosphere dynamics based on the oceanic advection of spiciness anomalies from the subtropics to the equator. Upon reaching the equator, these spiciness anomalies are upwelled to the surface where they create equatorial sea surface temperature anomalies which in turn produce a fast atmospheric response responsible for changing the sign of the subtropical spiciness anomalies and reversing the phase of the cycle.

Existing studies largely concentrate on the generation of annual and interannual spiciness anomalies (e.g., Yeager and Large, 2004; Kolodziejczyk and Gaillard, 2012, 2013), whereas the present study focuses on decadal spiciness anomalies. Also, the aforementioned studies investigate the spiciness generation through convective mixing, while this study is based on spiciness generation through anomalous advection across mean spiciness gradients. It is currently unclear what the relative proportion of the two generation mechanisms is. In fact, Kolodziejczyk and Gaillard (2012) state that decadal spiciness anomalies seem not to be associated with the convective mixing mechanism, which suggests other processes like the underlying spiciness generation mechanism in the present study to be at play.

However, it is still unclear if spiciness anomalies can persist from the source region to the Eastern equatorial Pacific where they potentially upwell and interact with the atmosphere. Another contentious question is whether spiciness anomalies travel to the tropical Pacific via the Western boundary as suggested by Schneider (2000), Giese et al. (2002), and Yeager and Large (2004) or if they propagate through the interior ocean as suggested by Li et al. (2012) and Thomas and Fedorov (2017). In the present study, we aim to shed light on the pathway of the subtropical to tropical exchange and the potential contribution of the "spiciness mechanism" to tropical Pacific decadal variability using a high resolution ocean general circulation model (OGCM) along with a Lagrangian particle simulator.

The paper is structured as follows: section 2 details the OGCM and the Lagrangian tracer model as well as the Lagrangian tracer experiments that have been carried out. Section 3 describes the occurrence and pathways of spiciness anomalies. A discussion and conclusions are provided in section 4.

## 2 Model and Methods

### 2.1 The Ocean Model

We use a global coupled ocean sea-ice model (GFDL-MOM025) which is based on the GFDL CM2.5 coupled climate model (Delworth et al., 2012) and is coupled to the GFDL Sea Ice Simulator model. The GFDL-MOM025 model has a 1/4 Mercator horizontal resolution globally and 50 vertical levels. The vertical level thicknesses range from 10 m at the surface to about 200 m at depth. Sea surface salinity is restored to a seasonally varying climatology on a 60 day time scale. To reach steady-state conditions in the upper ocean, the model is forced with the ERA-interim climatology of heat, freshwater and momentum fluxes in a 40 year spin-up control simulation. The OGCM resolves mesoscale variability in the tropics and subtropics and the use of 5-day average output enables us to reliably include the spatially complex transport of tracers by mesoscale eddies.

After the spin-up simulation, the ocean model is forced with climatological heat and freshwater fluxes and a fully varying wind field derived from the ECMWF ERA-interim reanalysis product (Dee and Uppala, 2009) that extends from January 1979 to May 2016. The ERA-interim winds were selected to overcome the strong trend biases in wind stress and wind stress curl over the tropical Pacific that are known to be present in the NCEP/NCAR (National Centers for Environmental Prediction/National Center for Atmospheric Research) wind product (McGregor et al., 2012). While this choice moved us away from the more balanced fluxes of CORE (Coordinated Ocean-ice Reference Experiments) forcing (Large and Yeager, 2009), the more realistic wind stress forcing appears to be more appropriate to address the proposed research questions.

### 2.2 Decadal Spiciness Variability

We define spiciness as temperature on isopycnal surfaces. This is equivalent to choosing salinity on the same surfaces, as by definition they show the same behaviour. The mean spiciness distribution is characterised by two zonal lobes of spiciness maxima, one in each hemisphere, stretching from the west to the east. The SH lobe is clearly warmer than the NH lobe with SH temperatures reaching up to 25 C compared to 21 C in the NH. The mean spiciness structure agrees well with Argo observations (Figure 1a). Based on Argo floats, Yeager and Large (2007) and Li et al. (2012) identified the subtropical Northeastern and Southeastern Pacific as prominent regions for the generation of strong spiciness anomalies during winter. Consistent with these observations, we find the strongest variance of modelled spiciness in the Northeastern and Southeastern subtropical Pacific (Figure S1).

We focus on the spiciness anomalies in the eastern/central equatorial Pacific where spiciness anomalies are thought to upwell after their advection from the subtropics. Averaging over the equatorial region (EQbox, 160 E-100 W, 2 S-2 N, Figure 1a) we find the strongest decadal spiciness signal to emerge on the $_{24}$ to $_{25.5}$ isopycnal surfaces (Figure 1b). This is also the range of isopycnals that Schneider (2000) found to exhibit the strongest decadal changes in spiciness. Furthermore,

extratropically generated spiciness anomalies on the $_{24}$ isopycnal surface do not reach the tropics as they stay relatively close to the surface and are thus strongly affected by the seasonal outcropping of isopycnals (not shown). We therefore restrict our analysis to the $_{24.5}$, $_{25}$, and $_{25.5}$ isopycnal surfaces. We identify two positive peaks (POS1, POS2) with anomalous isopycnal layer temperatures of up to +0.33 C and +0.16 C, respectively, and one negative peak (NEG) with anomalous temperatures of down to -0.17 C (Figure 1b). In the following, we are seeking to identify the source regions of the contributing spiciness anomalies by back-tracking particles from the equatorial region.

## 2.3 The Lagrangian Particle Simulator

To follow the potential pathways of the spiciness anomalies through the ocean we make use of the OceanParcels Lagrangian particle simulator (Lange and Sebille, 2017). Using a fourth order Runge-Kutta time integration OceanParcels allows us to simulate the trajectories of virtual particles through space and time. As by definition spiciness anomalies can only travel along isopycnal surfaces, we convert the 5-day average ocean model output (horizontal velocities, temperature, salinity) from Cartesian coordinates to density coordinates by linear interpolation onto pre-defined density surfaces. Particles are therefore tracked on 2-D isopycnal surfaces. The tracer simulations are computed off-line and use the ocean model 5-day average horizontal velocities. We also sample the hydrographic field along the particle trajectories which enables us to readily monitor the evolution of temperature, salinity and depth of each particle.

## 2.4 The Tracer Experiments

Particle sets, which behave like passive tracers akin to spiciness anomalies, are released in the EQbox region on the selected isopycnal surfaces ( $_{24.5}$, $_{25}$ , $_{25.5}$) during the identified periods of strong spiciness anomalies. Each particle set contains 3,417 particles with particles being released between 160 E and 100 W in 0.5 increments and between 2 S and 2 N in 0.25 increments. Particle sets are released every 3 months during the 3-year time span surrounding each decadal spiciness peak (POS1, POS2, NEG), which amounts to 12 different release dates for each peak. This results in 41,004 particles per decadal spiciness peak on each isopycnal surface. As we consider three isopycnal surfaces, the total number of particles for each decadal spiciness peak is 123,012. The procedure of having multiple release dates for each decadal peak increases the number of particles tracked and also ensures that the particle trajectories are independent of the exact release date. We find this to be a reasonable trade-off between the number of particles released and computational e ciency. For comparison, a reference particle set (REF) is released at 41 release dates in between the identified decadal spiciness peaks. The REF release dates were distributed across the entire time period to ensure independence between release dates and thus increase the number of degrees of freedom when calculating the significance of the changes in the other experiments. For all experiments, each particle set is tracked backward in time for 10 years on

daily time steps. Particle positions, spiciness and other properties are saved every month. As spiciness anomalies lose their characteristic as a passive tracer once they are upwelled into the mixed layer and come into contact with the atmosphere, in the following we consider only those particles which have not yet crossed the temporally and spatially varying mixed layer depth (MLD) as they are advected backward in time. The MLD is an output variable of the OGCM and is determined by density criteria. To account for the effect of subgrid-scale advection through baroclinic eddies, we apply horizontal Brownian diffusion to the advection scheme. According to Okubo (1971), diffusivities of 10-100 $\frac{m^2}{s}$ are representative for turbulent diffusion at spatial scales of 10-100 km, respectively. In consideration of our model resolution with a grid cell length of $\sim$25 km, we choose a default diffusivity of 10 $\frac{m^2}{s}$. In a more recent estimate, Ruehs et al. (2018) suggests a diffusivity of about 300 $\frac{m^2}{s}$ for the same length scale. We, therefore, test the sensitivity of our results to the chosen value of diffusivity (see section 3.3) and our conclusions appear to be insensitive to this choice.

## 3 Results

### 3.1 Subtropical-Tropical Water Pathways

As a first step we focus on the pathways of water parcels propagating between the subtropics and the tropics. To this end, we apply the condition that particles originating in the equatorial region have to cross 10  latitude at some point during their trajectory, while all other particles are disregarded. We also distinguish between four pathways for the advection of particles from the subtropics to the equator: the Western boundary and the interior pathway in both the Northern and Southern hemispheres. To be classified as a NH (SH) western boundary pathway, particles have to pass through the NH (SH) WBC box (cf. Figure 1 c) and 10 N (10 S). Particles that cross 10  latitude outside of the respective WBC box are classified as travelling on the interior pathway.

Before analysing the individual equatorial spiciness events, the aim of this section is to examine the average Lagrangian pathways. We therefore consider the composite of all experiments for this case. In our time frame of 10 years, 75% of all particles arriving at the equator have their origin in the subtropics (Figure 2, black numbers in Table 1) while the remaining 25% come from within the tropics. Half of all particles enter the tropics from the SH while a quarter enters from the NH. This preference for the SH pathways is consistent with the existence of the potential vorticity barrier between 10-15 N which inhibits the exchange of water from the subtropics to the tropics through the interior (Lu and McCreary Jr, 1995). The SH exchange displays a clear preference for particles to enter the equatorial region via the interior pathway (with the interior transports typically being 50% larger than the WBC transports), while both pathways are generally of equal prominence in the NH.

## 3.2 Advection of Spiciness Anomalies

In this section, we investigate the existence of the so-called "spiciness mechanism". According to this mechanism, spiciness anomalies that are generated in the subtropics are advected to the equator where they upwell into the mixed layer and imprint on the decadal SST variability. Thus, from here on, we only consider the 75% of particles that have their origin outside the tropics as described in the previous section. Furthermore, we now also take into account the spiciness (temperature) anomalies that these water parcels carry to assess and quantify the relative importance of the four pathways and their impact on the EQbox decadal spiciness anomalies. To this end, another condition is applied to the particles in addition to the ones that determine the pathway as described in the previous section. According to this new condition, particles have to keep a temperature anomaly of at least +0.1 C for the positive peaks and -0.1 C for the negative peak, from where they are generated outside the tropics until they reach the equatorial box. All other particles are not considered remotely generated spiciness anomalies. We choose the 0.1 C threshold as this is the average decadal spiciness anomaly at the equator for POS2 and NEG. For POS1, the average decadal spiciness anomaly reaches up to 0.3 C. However, to be consistent and facilitate comparability we apply the same threshold for all three experiments. Applying this additional condition affects the relative importance of the resulting pathways differently for the different experiments. Therefore, investigating the composite of all experiments is not legitimate in this case.

### *3.2.1 Positive spiciness anomalies*

Table 1 reveals that POS1 is clearly the most e cacious experiment when it comes to the advection of spiciness anomalies. More than 25% of all particles released in POS1 maintain their spiciness anomaly and are sourced from outside the tropics. This is equivalent to more than one third of all particles that are sourced from outside the tropics maintaining their spiciness anomaly. In POS1, it is evident that the SH plays a much more important role in carrying subtropical spiciness anomalies to the EQbox region than the NH (Figure 3). The combined percentage of particles carrying spiciness anomalies from the NH subtropics to the tropics is 2.6%, which is roughly 10% of the magnitude of the SH (Table 1). The overall dominant pathway is the SH interior which accounts for up to 16.6% of all particles released, equalling to more than half of the particles following the SH interior pathway, and also equalling to two thirds of all particles maintaining their spiciness anomaly.

On average, water parcels take about 4 years to propagate from the SH eastern subtropical Pacific to the EQbox region via the interior pathway, and about 6 years when they propagate via the WBC (Figure 3 c and d). The $25^{th}$ and $75^{th}$ percentiles of the particle propagation time deviate from the median by about 1-1.5 years. These reported propagation times are in line with previous findings (Schneider, 2000).

The temporal evolution of the POS1 spiciness anomalies from their source region to the equator exhibits a gradual decrease along the interior pathways from about 0.8 C to about 0.4 C and a rather constant value of about 0.4 C along the NH and

SH WBC (Figure 4, thick red line). The evolution suggests that particles are more prone to lose their spiciness anomaly when they travel along the interior while particles largely preserve their spiciness anomaly along the WBC pathway. Part of the explanation is given by the spatial distribution of the temperature anomalies along each pathway (Figure S7). The distribution shows that for the interior pathways subtropical spiciness anomalies are rather generated within the region of strongest spiciness variability, i.e. spiciness anomalies have a comparatively high magnitude. Spiciness anomalies following the WBC pathway, on the other hand, tend to be generated outside the main area of strongest spiciness variance and therefore are smaller from the start (cf. Figure 4 and Figure S7).

Along with the evolution of averaged spiciness anomalies, the evolution of the number of particles maintaining spiciness anomalies also has to be considered. In the Northern hemisphere, Figure 5 shows a gradual increase in the number of POS1 particles from the source region to the EQbox. However, the total numbers are comparatively small amounting to about 10% of each pathway's particles when they arrive at the tropics (vertical lines in Figure 5). Thus, despite the NH spiciness anomalies being large greater than six years before arrival at the equator, their effect on the average temperature is relatively small (Figure 4 top, thin solid red lines). In the Southern hemisphere, the number of particles maintaining spiciness anomalies increases gradually along the WBC pathway, with values larger than the NH counterpart, indicating a constant generation of spiciness anomalies along the way. The number of particles for the SH interior pathway exhibits a remarkably strong increase between 1-3 years before arriving at the equator (Figure 5). This strong increase coincides with the time when particles are at the spiciness outcropping region in the Southeastern subtropics (cf. Figure 1c). Note that as the term "outcropping region" is utilised when back-tracking spiciness anomalies, in reality, this likely represents a region of spiciness anomaly generation. The thin lines in Figure 4 show the temperature anomaly averaged over all particles for a given pathway, also including spiciness anomalies that decay before arriving at the equator. The thick line, in contrast, only shows the average over the spiciness anomalies that maintain their temperature anomaly along the pathway until they reach the equator. As the majority of particles lose their temperature anomaly (cf. Figure 5), i.e. have very small or negative anomalies, the average (thin line) were expected to be close to zero. However, the existence of larger positive spiciness anomalies drags the thin line away from zero towards positive values. Thus, comparing the thin to the thick line reveals that the subtropical spiciness anomalies of all regions have an effect on the total spiciness anomaly in POS1. The SH interior pathway is still expected to be dominant as the proportion of transport coming from this region is much larger compared to the other pathways (Figure 3).

It has to be noted that the increase in the number of spiciness anomalies seen in Figure 5 does not have to go along with an increase in the magnitude of the spiciness anomalies. On the contrary, a large number of small spiciness anomalies being added to existing large spiciness anomalies leads to a decrease of the average magnitude of spiciness anomalies along the way. In fact, the decrease in the average magnitude of spiciness anomalies seen in Figure 4 is partly explained by this effect.

In POS2 which is a clearly smaller anomaly than POS1, only 3.6% of the particles carry their spiciness anomaly from the subtropics to the equator (Table 1 and Figure 5). Roughly two thirds of these particles propagate via the SH WBC and one third via the SH interior (Figure S6). However, given the low percentage their contribution to the equatorial heat content is negligible as can be inferred from comparing the thin with the thick magenta line in Figure 4. This comparison shows that the subtropical spiciness anomalies (thick lines) have no effect on the total spiciness anomaly averaged over all particles (thin lines) which is mostly hovering around zero. The spatial distribution of the temperature anomalies along each pathway is depicted in Figure S8 and confirms that the spiciness anomalies are not generated in the region of strongest spiciness variance and are thus comparatively small.

#### *3.2.2 Negative spiciness anomalies*

In the case of NEG, where particles carry a negative temperature anomaly, 11.1% maintain their anomaly from the subtropics to the equator (Figure 6). In total, half of the spiciness anomalies are sourced from the Northern hemisphere and the other half from the Southern hemisphere (Table 1). Interestingly, negative spiciness anomalies during this event preferably propagate along the NH WBC (5.3%) while the NH interior only carries a very small amount (0.2%). The SH contribution is partitioned into 3% via the SH interior and 2.6% via the SH WBC. In terms of the temporal evolution of the anomalies (Figure 4, blue line), the spiciness anomalies largely stay at a constant value. However, for the NH WBC pathway the temperature anomaly almost doubles from about -0.4 C to -0.8 C during the last year before arriving at the equator. The spatial distribution of the temperature anomalies along the pathways (Figure S9) reveals that the remotely generated spiciness anomalies grow as they pass the far west equatorial Pacific. This is a region of strong mixing related to the stationary Mindanao eddy which could contribute to the rapid increase in the magnitude of the spiciness anomalies that follow the NH WBC pathway.

The number of NEG spiciness anomalies increases gradually along the NH WBC pathway (Figure 5a, blue line) and along the SH interior pathway (Figure 5d), again indicating spiciness generation along the way as for POS1. In contrast to POS1, there is no substantial rise along the SH interior pathway during years 1-3 before arriving at the equator (Figure 5d). For both the NH interior and the SH WBC pathways, the number of NEG spiciness anomalies is below 1% at the time they reach the tropics (Figure 5 b and c).

### 3.3 Alternative Generation of Equatorial Pacific Decadal Spiciness Anomalies

The previous section has investigated the propagation of decadal spiciness anomalies from their generation region in the subtropics to the equator. The decadal spiciness signal in that case is assumed to be a result of the advection of remotely generated spiciness anomalies. However, as illustrated by the POS2 experiment,

remotely generated spiciness anomalies are not the only contributor to the equatorial spiciness signal. Even though there is a clear decadal peak in equatorial Pacific subsurface spiciness, the contribution from remotely generated spiciness anomalies advected to the region is negligible. Our results suggest that processes within the equatorial band are responsible for generating local spiciness anomalies. We here propose two alternative generation mechanisms that can explain the POS2 spiciness peak. The first mechanism is that these anomalies are generated through local anomalous advection across mean temperature gradients on isopycnals, just like remotely generated spiciness anomalies. The second mechanism we propose is that these tropically generated spiciness anomalies result from the hemispheric differences in the mean spiciness distribution in the Pacific (Figure 1a). Mean temperature differences are seen of up to 4 C between the Northern and Southern hemisphere on the same isopycnal surface, in particular towards the eastern side of the basin which features the primary region for the generation of spiciness anomalies. Consequently, a changing proportion of NH versus SH equatorward transport would lead to the generation of spiciness anomalies when the two water masses are mixed once they join the equatorial undercurrent; i.e., an increased contribution from the NH (SH) waters would lead to a negative (positive) peak in spiciness at the equator.

In fact, our analysis of the back-tracking experiments provides evidence that supports this idea. The examination of the four experiments reveals some relatively small but discernible differences in the particle density distribution indicating the relative importance of each pathway (black numbers in Table 1, Figures S2-S5). In this regard, the NH interior contribution is particularly weak during the POS1 period resulting in a decreased NH versus SH ratio and promoting an increased importance of the warmer SH spiciness. On the other hand, the NH WBC contribution is particularly strong during the NEG period leading to an increased NH versus SH ratio and associated larger contribution of colder spiciness. This mechanism will be further discussed in section 4.

### 3.4 Sensitivity to Horizontal Diffusion Coe cient

We have tested the sensitivity of the advection of particles to different diffusion coe cients (Table 2). The results indicate that with increasing diffusivity the percentages of the WBC pathways generally increase, except for the SH WBC pathway at a diffusivity of 1000 $\frac{m^2}{s}$. This relationship applies to both plain water parcels and spiciness anomalies. The increased percentages result from an increased spatial radius of probability for the location of each particle during the advection. This radius increases with a higher diffusion. As a consequence, at a higher rate of diffusion the probability that particles can cross 10 latitude increases. Interestingly, diffusion does not appear to impact the interior pathways given the negligibly small changes, except for the increase of the NH interior pathway at a diffusivity of 1000 $\frac{m^2}{s}$. This is thought to be related to the smaller spatial temperature gradients in the interior as compared to the western boundary which inhibits diffusion even at high diffusivity values.

While we do not have an explanation for the reduced percentage of the SH WBC

pathway at a diffusivity of 1000 $\frac{m^2}{s}$, the sensitivity analysis shows that our conclusions are not sensitive to the chosen value of diffusivity. As the percentages in our default case are somewhere in the mid of the range, we believe that $\kappa$=10 $\frac{m^2}{s}$ is a reasonable value for the diffusion coe cient.

## 4 Discussion and Conclusions

The motivation of this study was to clarify whether spiciness anomalies generated in the subtropical Pacific can propagate with the ocean currents to the equator with significant amplitude. We therefore applied a Lagrangian particle simulator which uses the output of a high-resolution OGCM to back-track virtual spiciness anomalies from the equator at periods of equatorial spiciness peaks, namely POS1, POS2 and NEG. The present study provides a quantitative assessment of the relative contribution of different pathways to the transport of water and spiciness anomalies from the Pacific subtropics to the equator. We find that approximately 50% of the water arriving at the equator is sourced from the SH subtropics, one quarter is sourced from the NH subtropics, and the remaining quarter has its origin within the tropics (defined here as 10 S-10 N). These results are in very good agreement with the recent study by Nie et al. (2019) who found a subtropical to tropical ratio of 4/1. In their study, the authors further determined that the subtropical contribution primarily stems from the North and South Eastern subtropical mode waters, while the tropical contribution arises from the equatorially confined tropical cells. Similar to Nie et al. (2019), our results suggest an increasing contribution of the WBC (interior) water towards the western (eastern) equatorial undercurrent (Figure 2). Knowing the source regions of upper Pacific Ocean equatorial water emphasises the need of observations in the respective remote areas to better estimate the water properties which are advected to the equator. Information about the pathways further helps to better understand the mechanisms and predict the interannual to decadal climate of this region.

We could further demonstrate that remotely generated spiciness anomalies are able to propagate from the subtropics to the equator, while still maintaining a considerable fraction of their original temperature anomaly. As opposed to most previous studies these spiciness anomalies are generated by anomalous advection across mean spiciness gradients and are thus not dependent on the thermodynamic state of the atmosphere. For two out of the three case studies, namely POS1 and NEG, we find a considerable impact of subtropical spiciness anomalies for the formation of equatorial subsurface spiciness peaks. In the case of the positive peak in equatorial subsurface temperature in the early 1990s (POS1), almost all of the subtropical spiciness anomalies originate from the Southern hemisphere and the large majority of the SH spiciness anomalies (72%) travel via the interior pathway. This is in disagreement with previous studies suggesting that temperature anomalies travel via the western boundary pathways (Giese et al., 2002; Yeager and Large, 2004), while it corroborates the studies that propose the interior pathway to be the more dominant (Li et al., 2012; Thomas and Fedorov, 2017). This result is important as it implies a shortened lead time for the predictability of equatorial spiciness peaks because interior pathways on average have a two year shorter transit time (4-6 years) than the WBC pathways (6-8 years).

Further, our results for POS1 show a decrease of temperature anomalies over time for the interior pathways and no change for the WBC pathways (Figure 4, red line). A possible explanation for this is that spiciness anomalies propagating via the WBC pathways do not originate from further poleward than 20 latitude, whereas spiciness anomalies propagating via the interior pathways originate from as far poleward as 30 latitude (cf. Figure 3). Thus, early spiciness anomalies propagating via the interior pathway originate from the region with the strongest variance in spiciness (Figure S1) resulting in strong spiciness anomalies accordingly (Figure S7). Interestingly, once the POS1 spiciness anomalies arrive at the equator they tend to have similar magnitudes no matter which pathway they took.

In contrast to the positive peak in spiciness (POS1), which has its largest spiciness anomaly contribution from the SH interior, the negative spiciness peak (NEG) is primarily contributed to by spiciness anomalies following the NH WBC pathway (48%). As a consequence, the lead time for the potentially predictable cold equatorial spiciness signal is two years longer than that of POS1. It is unknown whether the hemispheric difference in spiciness contribution identified by POS1 and NEG is a symptom of some larger scale process, i.e. changes in the basin-wide Pacific background state on decadal to multi-decadal time scales.

A special case is given by POS2 in which case, the contribution of remotely generated spiciness anomalies is negligible. Nevertheless, there exists a warm spiciness peak at the equator. We propose that the signal is still remotely forced but not by the advection of spiciness anomalies, but by the changing proportion of NH versus SH advection of mean spiciness. Given the large differences in mean spiciness between both hemispheres (Figure 1a), deviations from the normal transport proportion lead to the generation of spiciness anomalies at the equator once the water masses merge and join the EUC. It should be noted here that while these spiciness anomalies are generated locally in the equatorial band, they are still forced remotely by the changing ratio of Northern hemisphere and Southern hemisphere source waters.

This consistency between the source hemisphere of the anomaly and the mean temperature of the hemisphere applies to all three case studies and is demonstrated by the ratio of Northern versus Southern hemisphere pathways (Figure 7). The ratio is clearly smaller for the two warm spiciness events (POS1, POS2) compared to the reference experiment (REF), which suggests that an anomalously large portion of warm equatorial waters comes from the Southern hemisphere. Moreover, the POS1 and POS2 ratios are outside the distribution of ratios derived from 10,000 times randomly subsampling 12 out of the 41 release dates of the REF experiment, highlighting the significance of the difference of these ratios from the reference ratio (Figure 7). Conversely, for the cold spiciness event the NH versus SH ratio is greater than for the REF experiment, although within the range of possible ratios for REF conditions, indicating that more equatorial water than usual originates from the Northern hemisphere. As mentioned before, this explanation mainly applies to the POS2 spiciness event where there is almost no contribution from remotely generated spiciness anomalies. By contrast, POS1 and NEG both show clear contributions from advected subtropical spiciness anomalies. The relevance of locally generated spiciness anomalies as described above remains

unclear and is subject to more data in the future.

As we utilise climatological heat fluxes to force the ocean, the generation mechanism through convective mixing at the base of the surface mixed layer is likely poorly represented. Instead, the majority of spiciness anomalies will be generated through anomalous advection across mean temperature gradients as explained in section 1. To assess the relative importance of the two spiciness generation mechanisms, a reference OGCM simulation has been performed forced with observed estimates of the fully varying atmospheric conditions (CORE2-IAF, Gri es et al. (2009); Large and Yeager (2009)). The spiciness generation regions (spatial correlation of 0.86) and the equatorial spiciness signals (correlation of 0.41) are to a large degree of a similar nature for both simulations (not shown). Therefore, the main message of the present study, namely the capability of spiciness anomalies to propagate from the subtropics to the equator, still prevails and might even be enhanced by additional large spiciness anomalies. Also, due to the design of our study we know that these anomalies must have been generated through anomalous advection across mean spiciness gradients and it will be interesting to more thoroughly explore the differences between our simulations and those of a CORE2-IAF forced OGCM simulation in a future study.

It has to be kept in mind that the length of the considered time period only allows us to investigate three decadal peaks. Therefore, we cannot claim statistical significance for the exact contributions of each pathway for the different experiments. It may be possible that the relative importance of the pathways will change for future peaks in subsurface equatorial spiciness. The integration time of 10 years for the Lagrangian back-tracking experiments may also have an effect on the results as spiciness anomalies that are generated longer than 10 years ago are not captured in our study. Thus, a further experiment with a longer integration time might add further insights into the generation regions of spiciness anomalies and their advection to the equator.

In terms of the robustness of the results, the largest uncertainty arises from the potential impact of diapycnal diffusion which is not considered in this study. Diapycnal diffusion can have a considerable impact on the magnitude of spiciness anomalies over time as observed by Johnson (2006), although their study only focuses on a single spiciness anomaly in the Southern hemisphere subtropics. An estimate of the uncertainty of the pathways is implicitly provided by the width of the pathways in the probability distribution maps in Figures 2, 3, and 6.

Finally, this study demonstrates that spiciness anomalies are able to be advected from the subtropics to the tropics while preserving a considerable fraction of their temperature anomaly. We further show that the ”spiciness mechanism” can act as an important contributor to large peaks of equatorial subsurface temperature. Under the assumption that large spiciness anomalies are upwelled along the equator and imprint on the equatorial SST, they may have an appreciable impact on the decadal variability of the tropical Pacific and thus constitutes a valid instrument of inducing TPDV. Assuming that spiciness anomalies make up a substantial portion of the equatorial SST variance, the lead time of spiciness advection may affect the predictability of the tropical Pacific climate as a whole. It has to be noted that the influence of spiciness anomalies on equatorial SST is currently unclear. Thus,

598 an intriguing next question is how big the actual impact of spiciness anomalies on
599 the tropical Pacific SST is on decadal time scales. We intend to address this ques-
600 tion in a follow-up study, where we will assess the contribution of these spiciness
601 anomalies to the equatorial Pacific mixed layer by carrying out a detailed heat
602 budget analysis.

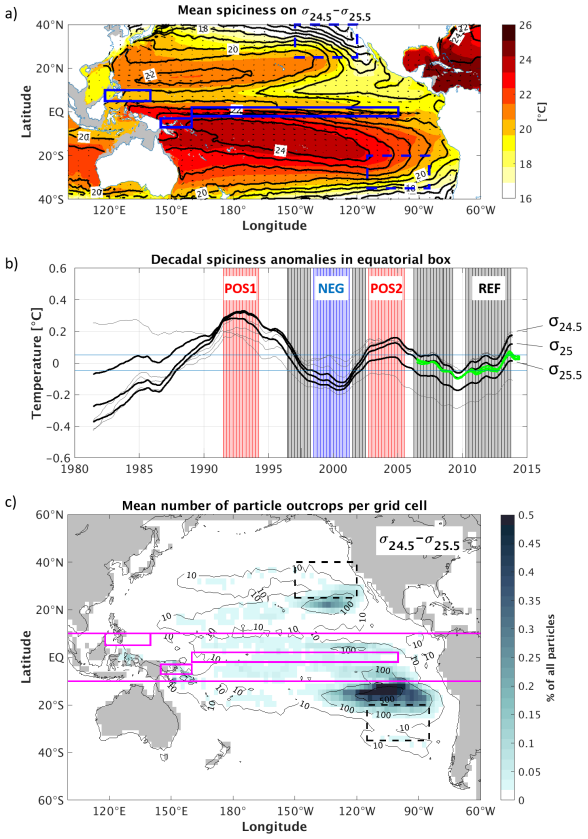


**Fig. 1** a) GFDL-MOM025 mean spiciness averaged over the $_{24.5}$, $_{25}$, and $_{25.5}$ surfaces. Black contours with white labels show Argo observations. The dashed boxes indicate the observed source regions of spiciness anomalies. The solid boxes at the western boundary are used to distinguish WBC pathways from interior pathways. The solid box along the equator indicates the region where spiciness anomalies emerge after they are advected from their source region. b) Evolution of spiciness anomalies averaged over the equatorial box on different isopycnal surfaces ranging from $_{23}$ to $_{26}$. The isopycnal layers $_{24.5}$ to $_{25.5}$ are highlighted as they show the strongest decadal variability. The green lines show Argo observations. A 5-year moving average has been applied to highlight low frequency changes. Overlying red, blue, and grey boxes/lines indicate the particle release periods/dates for the positive, negative, and neutral experiments, respectively. The thin horizontal lines indicate the 0.1 (-0.1) C threshold below (above) which spiciness anomalies are disregarded in the back-tracking analysis. c) Percentage of particle outcrops (particles crossing MLD) averaged over all experiments for all released particles. Contours indicate the number of outcropped particles.

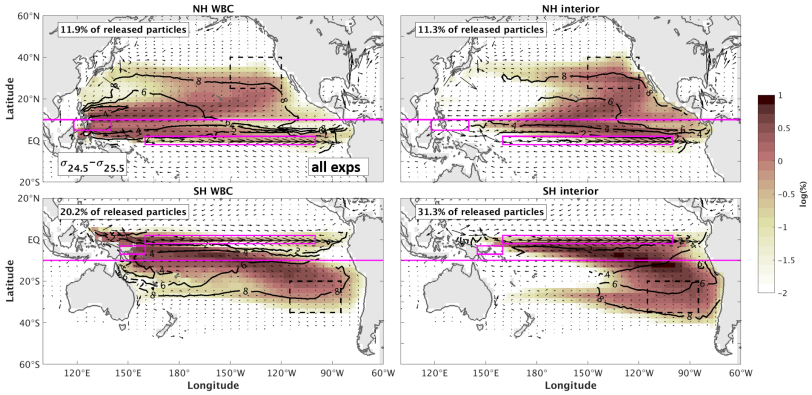


**Fig. 2** Tracer pathways on $_{24.5}$ $_{25.5}$ (all four experiments combined) along the different pathways: a) NH WBC, b) NH interior, c) SH WBC, d) SH interior. The boxes are the same as in Figure 1a. The shading indicates the particle density (percentage of particles that cross grid cell) to identify the pathways, with the colour scale being logarithmic, i.e. 1=10%, 0=1%, -1=0.1%. Overlying arrows show the time mean ocean current velocities averaged over the respective isopycnal surfaces. Black contours indicate the median travel time of particles in years. The relative contribution of each pathway is indicated as a percentage with respect to all particles crossing 10 latitude in the upper left corner of each panel.

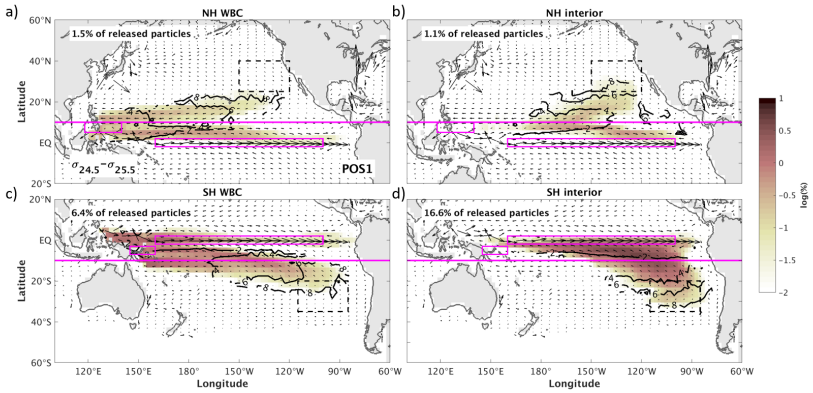


**Fig. 3** Same as Figure 2 but with the additional condition that spiciness anomalies of each tracer must not fall below 0.1 C. Shown is the POS1 experiment. Black contours indicate the median travel time of particles in years.

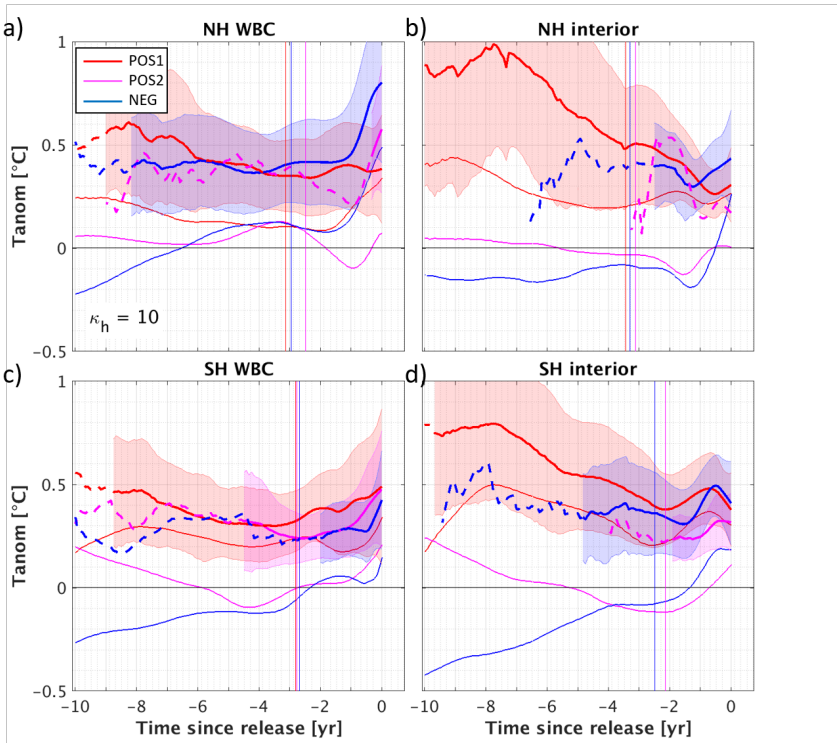


**Fig. 4** Temporal evolution of spiciness anomalies along the different pathways: a) NH WBC, b) NH interior, c) SH WBC, d) SH interior. The thick lines show the temperature anomaly averaged over all particles which maintain their spiciness anomaly for each pathway. The thin lines show the temperature anomaly averaged over all particles for each pathway. Note that NEG anomalies have been multiplied by -1. Thick lines become dashed when the number of particles is less than 1% relative to all particles of each pathway. The shading represents the particle spread (std) at each time step (only plotted when more than 1% of particles are apparent). The vertical lines indicate the average time when particles have reached 10 latitude.

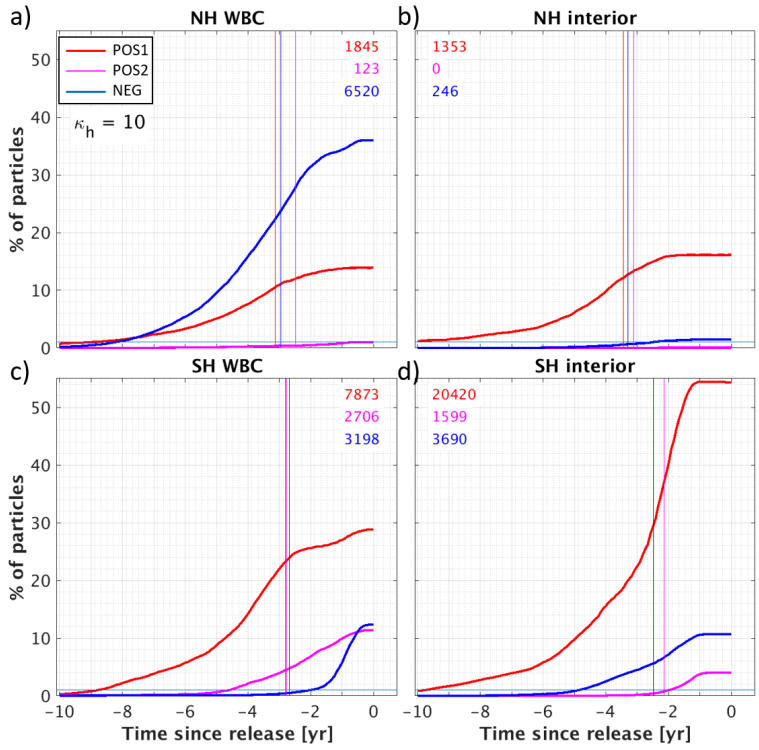


**Fig. 5** Temporal evolution of the percentage of particles maintaining their spiciness anomaly relative to all particles of each pathway: a) NH WBC, b) NH interior, c) SH WBC, d) SH interior. The total number of particles maintaining their spiciness anomaly for each pathway and experiment is noted in the top left/right corner of each panel. The horizontal line indicates the 1% mark. The vertical lines indicate the average time when particles have reached 10 latitude.

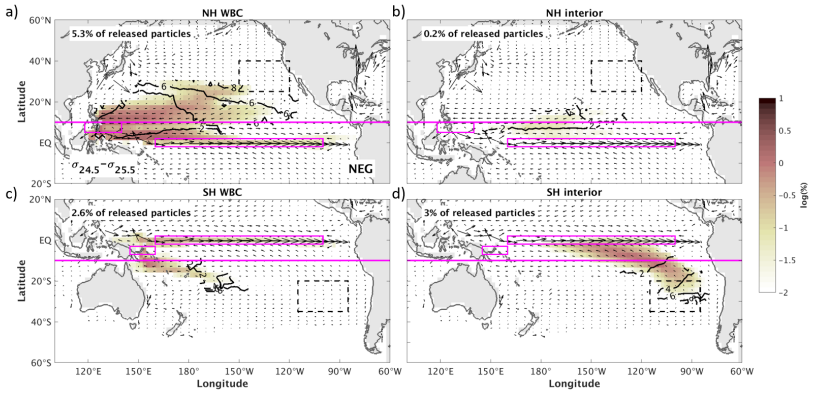


**Fig. 6** Same as Figure 3 but for NEG experiment.

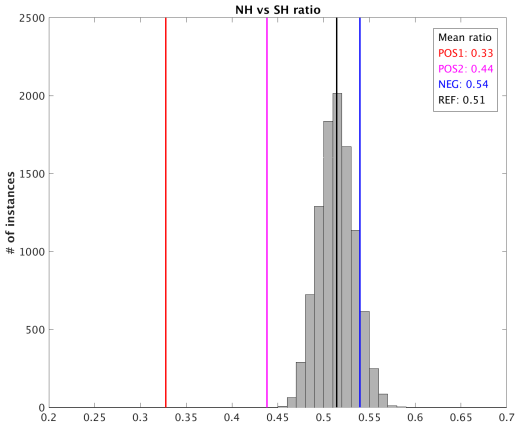


**Fig. 7** Ratio of NH versus SH contributions to equatorial water indicated as vertical lines for POS1 (red), POS2 (magenta), NEG (blue), and REF (black) experiments. The vertical lines indicate the mean ratio averaged over all release dates. The grey bars show the histogram of ratios derived from 10,000 random subsamples of 12 out of the 41 release dates for the REF experiment.

**Table 1** Percentage of particles following each pathway (**and maintaining their temperature anomaly**) for each experiment and the average over all experiment (AVG). Note that the bold numbers in AVG do not take into account the values of REF when taking the average.

| | NH WBC | SH WBC | NH interior | SH interior | NH total | SH total | SUM |
|---|---|---|---|---|---|---|---|
| POS1 | 10.9 (**1.5**) | 23.2 (**6.4**) | 6.5 (**1.1**) | 30.5 (**16.6**) | 17.4 (**2.6**) | 53.7 (**23**) | 71.1 (**25.6**) |
| POS2 | 11 (**0.1**) | 21.5 (**2.2**) | 11.6 (**0**) | 30.3 (**1.3**) | 22.6 (**0.1**) | 51.8 (**3.5**) | 74.4 (**3.6**) |
| NEG | 14.8 (**5.3**) | 18.3 (**2.6**) | 11.4 (**0.2**) | 30.7 (**3**) | 26.2 (**5.5**) | 49 (**5.6**) | 75.2 (**11.1**) |
| REF | 10.8 (**0**) | 18 (**0**) | 15.7 (**0**) | 33.7 (**0**) | 26.5 (**0**) | 51.7 (**0**) | 78.2 (**0**) |
| AVG | 11.9 (**2.3**) | 20.2 (**3.7**) | 11.3 (**0.4**) | 31.3 (**7**) | 23.2 (**2.7**) | 51.5 (**10.7**) | 74.7 (**13.4**) |

**Table 2** Percentage of particles following each pathway (**and maintaining their temperature anomaly**) for different horizontal diffusion coe cients $\kappa$ $[\frac{m^2}{s}]$.

| POS1 | NH WBC | SH WBC | NH interior | SH interior | SUM |
|---|---|---|---|---|---|
| κ = 0 | 7.7 (**1.2**) | 17.5 (**4.3**) | 6.5 (**1.1**) | 30.4 (**16.7**) | 62.1 (**23.3**) |
| κ = 10 | 10.9 (**1.5**) | 23.2 (**6.4**) | 6.5 (**1.1**) | 30.5 (**16.6**) | 71.1 (**25.6**) |
| κ = 100 | 12.1 (**1.9**) | 25 (**7.2**) | 6.6 (**1.2**) | 30.2 (**16.4**) | 73.9 (**26.7**) |
| κ = 1000 | 14.9 (**2.6**) | 21.8 (**5.6**) | 8.2 (**2.2**) | 30.3 (**16**) | 75.2 (**26.4**) |

**Acknowledgements** This study was supported by the Australian Research Council (ARC) through grants FT160100162 and FT190100413, with additional support coming via the ARC Centre of Excellence in Climate System Science and the ARC Centre of Excellence in Climate Extremes. The model integrations were performed at the Australian National Computing Infrastructure (NCI) Facility. The ocean model output is available from the NCI facility.

## Conflict of interest

The authors declare that they have no conflict of interest.

## References

Barnett, T., Pierce, D., Latif, M., Dommenget, D., and Saravanan, R. (1999). Interdecadal interactions between the tropics and midlatitudes in the Pacific basin. *Geophysical Research Letters*, 26(5):615–618. cited By 151.

Capotondi, A., Alexander, M., Deser, C., and McPhaden, M. (2005). Anatomy and decadal evolution of the Pacific Subtropical-Tropical Cells (STCs). *Journal of Climate*, 18(18):3739–3758. cited By 32.

Chikamoto, Y., Mochizuki, T., Timmermann, A., Kimoto, M., and Watanabe, M. (2016). Potential tropical Atlantic impacts on Pacific decadal climate trends. *Geophysical Research Letters*, 43(13):7143–7151. cited By 6.

Dee, D. and Uppala, S. (2009). Variational bias correction of satellite radiance data in the ERA-Interim reanalysis. *Quarterly Journal of the Royal Meteorological Society*, 135(644):1830–1841. cited By 270.

Delworth, T., Rosati, A., Anderson, W., Adcroft, A., Balaji, V., Benson, R., Dixon, K., Gri es, S., Lee, H.-C., Pacanowski, R., Vecchi, G., Wittenberg, A., Zeng, F., and Zhang, R. (2012). Simulated climate and climate change in the GFDL CM2.5 high-resolution coupled climate model. *Journal of Climate*, 25(8):2755–2781. cited By 110.

Di Lorenzo, E., Liguori, G., Schneider, N., Furtado, J., Anderson, B., and Alexander, M. (2015). ENSO and meridional modes: A null hypothesis for Pacific climate variability. *Geophysical Research Letters*, 42(21):9440–9448. cited By 2.

England, M., Mcgregor, S., Spence, P., Meehl, G., Timmermann, A., Cai, W., Gupta, A., Mcphaden, M., Purich, A., and Santoso, A. (2014). Recent intensification of wind-driven circulation in the Pacific and the ongoing warming hiatus. *Nature Climate Change*, 4(3):222–227. cited By 391.

Freund, M., Henley, B., Karoly, D., McGregor, H., Abram, N., and Dommenget, D. (2019). Higher frequency of Central Pacific El Niño events in recent decades relative to past centuries. *Nature Geoscience*, 12(6):450–455. cited By 1.

Giese, B., Urizar, S., and Fuckar, N. (2002). Southern hemisphere origins of the 1976 climate shift. *Geophysical Research Letters*, 29(2):1–1. cited By 91.

Gri es, S., Biastoch, A., Böning, C., Bryan, F., Danabasoglu, G., Chassignet, E., England, M., Gerdes, R., Haak, H., Hallberg, R., Hazeleger, W., Jungclaus, J., Large, W., Madec, G., Pirani, A., Samuels, B., Scheinert, M., Gupta, A., Severijns, C., Simmons, H., Treguier, A., Winton, M., Yeager, S., and Yin, J. (2009). Coordinated Ocean-ice Reference Experiments (COREs). *Ocean Modelling*, 26(1-2):1–46. cited By.

Gu, D. and Philander, S. (1997). Interdecadal climate fluctuations that depend on exchanges between the tropics and extratropics. *Science*, 275(5301):805–807. cited By 0.

Hazeleger, W., Visbeck, M., Cane, M., Karspeck, A., and Naik, N. (2001). Decadal upper ocean temperature variability in the tropical Pacific. *Journal of Geophysical Research: Oceans*, 106(C5):8971–8988. cited By 38.

Johnson, G. (2006). Generation and initial evolution of a mode water $\theta$-S anomaly. *Journal of Physical Oceanography*, 36(4):739–751. cited By 32.

Kleeman, R., McCreary Jr., J., and Klinger, B. (1999). A mechanism for generating ENSO decadal variability. *Geophysical Research Letters*, 26(12):1743–1746. cited By 205.

Kolodziejczyk, N. and Gaillard, F. (2012). Observation of spiciness interannual variability in the Pacific pycnocline. *Journal of Geophysical Research: Oceans*, 117.

Kolodziejczyk, N. and Gaillard, F. (2013). Variability of the Heat and Salt Budget in the Subtropical Southeastern Pacific Mixed Layer between 2004 and 2010: Spice Injection Mechanism. *Journal of Physical Oceanography*.

Kosaka, Y. and Xie, S.-P. (2013). Recent global-warming hiatus tied to equatorial Pacific surface cooling. *Nature*, 501(7467):403–407. cited By 272.

Lange, M. and Sebille, E. (2017). Parcels v0.9: Prototyping a Lagrangian ocean analysis framework for the petascale age. *Geoscientific Model Development*, 10(11):4175–4186. cited By 7.

Large, W. and Yeager, S. (2009). The global climatology of an interannually varying air - Sea flux data set. *Climate Dynamics*, 33(2-3):341–364. cited By.

Lee, T. and Fukumori, I. (2003). Interannual-to-decadal variations of tropical-subtropical exchange in the Pacific Ocean: Boundary versus interior pycnocline transports. *Journal of Climate*, 16(24):4022–4042. cited By 63.

Li, Y., Wang, F., and Sun, Y. (2012). Low-frequency spiciness variations in the tropical Pacific Ocean observed during 2003-2012. *Geophysical Research Letters*, 39(23). cited By 19.

Liu, Z., Philander, S., and Pacanowski, R. (1994). A GCM study of tropical-subtropical upper-ocean water exchange. *Journal of Physical Oceanography*, 24(12):2606–2623. cited By 152.

Lu, P. and McCreary Jr, J. (1995). Influence of the ITCZ on the flow of thermocline water from the subtropical to the equatorial Pacific Ocean. *Journal of Physical Oceanography*, 25(12):3076–3088. cited By 86.

McCreary Jr, J. and Lu, P. (1994). Interaction between the subtropical and equatorial ocean circulations: the subtropical cell. *Journal of Physical Oceanography*, 24(2):466–497. cited By 346.

McGregor, S., Gupta, A., and England, M. (2012). Constraining wind stress products with sea surface height observations and implications for Pacific Ocean sea level trend attribution. *Journal of Climate*, 25(23):8164–9176. cited By 54.

McGregor, S., Timmermann, A., Stuecker, M., England, M., Merrifield, M., Jin, F.-F., and Chikamoto, Y. (2014). Recent Walker circulation strengthening and Pacific cooling amplified by Atlantic warming. *Nature Climate Change*, 4(10):888–892. cited By 104.

Munk, W. (1981). Internal waves and small scale processes. *Evolution of Physical Oceanography, B. A. Warren and C. Wunsch, Eds., MIT Press, 264–291.*

694 Neske, S. and McGregor, S. (2018). Understanding the Warm Water Volume
695 Precursor of ENSO Events and its Interdecadal Variation. *Geophysical Research*
696 *Letters*, 45(3):1577–1585. cited By 0.
697 Newman, M., Alexander, M., Ault, T., Cobb, K., Deser, C., Di Lorenzo, E.,
698 Mantua, N., Miller, A., Minobe, S., Nakamura, H., Schneider, N., Vimont, D.,
699 Phillips, A., Scott, J., and Smith, C. (2016). The Pacific decadal oscillation,
700 revisited. *Journal of Climate*, 29(12):4399–4427. cited By 101.
701 Nie, X., Gao, S., Wang, F., Chi, J., and Qu, T. (2019). Origins and Pathways of
702 the Pacific Equatorial Undercurrent Identified by a Simulated Adjoint Tracer.
703 *Journal of Geophysical Research: Oceans*, 124(4):2331–2347. cited By 0.
704 Okubo, A. (1971). Oceanic diffusion diagrams. *Deep-Sea Research and Oceano-*
705 *graphic Abstracts*, 18(8):789–802. cited By 669.
706 Rodgers, K., Friederichs, P., and Latif, M. (2004). Tropical Pacific decadal vari-
707 ability and its relation to decadal modulations of ENSO. *Journal of Climate*,
708 17(19):3761–3774. cited By 156.
709 Ruehs, S., Zhurbas, V., Koszalka, I., Durgadoo, J., and Biastoch, A. (2018). Eddy
710 diffusivity estimates from Lagrangian trajectories simulated with ocean models
711 and surface drifter data-A case study for the greater Agulhas system. *Journal*
712 *of Physical Oceanography*, 48(1):175–196. cited By 3.
713 Schneider, N. (2000). A decadal spiciness mode in the tropics. *Geophysical Re-*
714 *search Letters*, 27(2):257–260. cited By 53.
715 Schneider, N., Miller, A., Alexander, M., and Deser, C. (1999a). Subduction of
716 decadal North Pacific temperature anomalies: Observations and dynamics. *Jour-*
717 *nal of Physical Oceanography*, 29(5):1056–1070. cited By 170.
718 Schneider, N., Venzke, S., Miller, A., Pierce, D., Barnett, T., Deser, C., and Latif,
719 M. (1999b). Pacific thermocline bridge revisited. *Geophysical Research Letters*,
720 26(9):1329–1332. cited By 58.
721 Schott, F., McCreary, J.P., J., and Johnson, G. (2004). Shallow overturning circula-
722 tions of the tropical-subtropical oceans. *Geophysical Monograph Series*, 147:261–
723 304. cited By 109.
724 Thomas, M. and Fedorov, A. (2017). The eastern subtropical pacific origin of the
725 equatorial cold bias in climate models: A Lagrangian perspective. *Journal of*
726 *Climate*, 30(15):5885–5900. cited By 5.
727 Vimont, D. (2005). The contribution of the interannual ENSO cycle to the spatial
728 pattern of decadal ENSO-like variability. *Journal of Climate*, 18(12):2080–2092.
729 cited By 57.
730 Yeager, S. and Large, W. (2004). Late-winter generation of spiciness on subducted
731 isopycnals. *Journal of Physical Oceanography*, 34(7):1528–1547. cited By 56.
732 Yeager, S. and Large, W. (2007). Observational evidence of winter spice injection.
733 *Journal of Physical Oceanography*, 37(12):2895–2919. cited By 32.
734 Zeller, M., McGregor, S., and Spence, P. (2019). Hemispheric asymmetry of the
735 Pacific shallow meridional overturning circulation. *Journal of Geophysical Re-*
736 *search: Oceans*.
737 Zhang, X., Sheng, J., and Shabbar, A. (1998). Modes of interannual and inter-
738 decadal variability of Pacific SST. *Journal of Climate*, 11(10):2556–2569. cited
739 By 48.
740 Zhao, M., Hendon, H., Alves, O., Liu, G., and Wang, G. (2016). Weakened Eastern
741 Pacific El Niño predictability in the early Twenty-First Century. *Journal of*
742 *Climate*, 29(18):6805–6822. cited By 6.